 ©2011 Kvantovaya Elektronika and Turpion Ltd

PACS numbers: 87.64.Cc; 87.63.L–; 42.30.Wb
DOI: 10.1070/QE2011v041n05ABEH014597

Using late arriving photons for diffuse optical tomography of biological objects

S.G. Proskurin

Dedicated to the memory of Britton Chance

Abstract. **The issues of detecting the inhomogeneities are studied aimed at mapping the distribution of absorption and scattering in soft tissues. A modification of the method of diffuse optical tomography is proposed for detecting directly and determining the region of spatial localisation of such absorbing and scattering inhomogeneities as a cyst, a hematoma, a tumour, as well as for measuring the degree of oxygenation or deoxygenation of blood, in which the late arriving photons that diffuse through the scattering object are used.**

Keywords: *diffuse optical tomography, time point spread function, late arriving photons, homogeneity index.*

1. Introduction

Diffuse optical tomography (DOT) can sometimes replace the X-ray computer tomography (CT) and nuclear magnetic resonance (NMR) tomography and sometimes is used as a complementary method of diagnostics. Though the CT and NMR provide perfect spatial resolution, they require rather cumbersome and expensive equipment. The DOT methods are substantially cheaper and more mobile and provide information about the oxygenation or deoxygenation of blood and about the functional condition of tissues.

The X-ray radiation is a hard and ionising radiation, dangerous for a living organism. Due to the quantum mechanical nature of the interaction, even small doses of X-ray radiation can cause mutations at the genetic level and lead to serious diseases.

In magnetic resonance tomography (MRT) the equipment is also cumbersome and the strong magnetic fields are used. The influence of such fields on the human organism is not studied completely; however, in the medical practice essential limitations are imposed on the value of magnetic induction (no greater than 4 Tesla).

Infrared spectroscopy and tomography are based on measuring the absorption and scattering spectra of optical radiation with the wavelength 700–1100 nm. More often they use the window 780–830 nm in the vicinity of the isosbestic point λ = 805 nm. Optical methods make use of safe and noninvasive ways of diagnostics, and the instrumentation for their implementation is much less cumbersome and much cheaper. In the future it is suggested to reduce the dimensions of the devices up to the size of a portable computer to provide convenient point-of-care diagnostics.

There are two methods of IR diffusion spectroscopy and tomography: the time-domain (pulse modulation tomography) [1–7] and the frequency-domain (frequency modulation tomography) [8, 9]. Obviously, the formulae, describing these two approaches, are related via the Fourier transform; however, in practice the use of the pulse-modulation approach provides certain advantages. The accumulation of the pulsed signal is equivalent to detecting a broad frequency band, theoretically, from zero to infinity. For example, the use of a 100-fs pulse is equivalent to the frequency region $0-10^{13}$ Hz. The instrumentation for the frequency-modulation tomography is cheaper and more compact, but the accumulation and processing of the signal take essentially more time.

In the time-domain tomography the registered quantity is the time-dependent intensity $R'(\alpha, t)$ of the ultrashort IR pulsed radiation, diffused through a scattering medium, referred to as time point spread function (TPSF) (Fig. 1). Here, α is the angle between the source and detector fibres. Usually most attention is paid to the initial part of the curve (region I, corresponding to early arriving photons) or its middle part (region II, determining the mean time of flight of a photon) [10]. However, it is possible to use also the last part of the time dependence of the diffused radiation (region III), corresponding to late arriving photons [11, 12]. It is important to note, that late arriving photons practically do not contribute to the

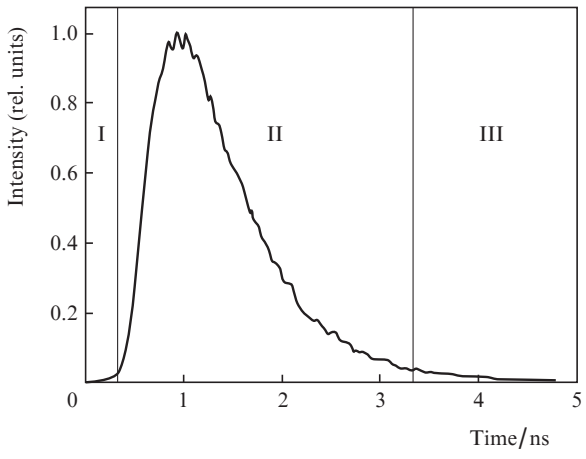

Figure 1. A typical view of TPSF for a scattering phantom with optical properties, similar to those of a biomedical object.

S.G. Proskurin Tambov State Technical University, ul. Sovetskaya 106, 392000 Tambov, Russia; e-mail: spros@tamb.ru

Received 25 February 2011; revision received 22 March 2011
Kvantovaya Elektronika **41** (5) 402–406 (2011)
Translated by V.L. Derbov

calculated mean time of flight of the photons diffusively travelled through the medium.

2. Formulation of the problem

The solution of the radiative transfer equation in the diffusion approximation for a cylinder and a sphere may be obtained in the analytical form [13]; however, for solving inhomogeneous problems of simulating hematomas, vascular neoplasms, or cancer tumours one should use 2D or 3D finite-element methods (2D, 3D FEM) [14–17].

A cylindrical or spherical phantom usually serves as a model object. At small distances between the source fibre and the detector fibre such an object may be treated as semi-infinite. It is traditionally agreed, that the major contribution to the signal, registered by the detector, comes from the banana-shaped region of the object [2, 3]. However, this is true only for early photons, while the middle part of the TPSF and the late arriving photons diffuse through the whole volume of the phantom and bring integral characteristics.

Analysing the experiments with real biological objects, whose scattering coefficient is $\mu_s' = 0.5–1.5$ mm^{-1}, one can conclude that there are almost no early photons that travel slightly declining from a straight line [4, 12]. The signal-to-noise ratio greater than 1 is realised in the diffusively scattered signal at delay times that are 2–3 times greater than the time of straight flight. Therefore, the detected signal of the first part of a TPSF covers from 50% to 80% of the object volume.

Theoretically it is possible to develop another integral approach, in which a virtual isotropic source (VIS) is formed at the depth, equal to the transport length $l^* = \mu_s'$ and moves from the surface to the centre of the object [18–21]. Developing this idea, it is possible to justify the use of late arriving photons for the frequency-domain tomography too, which may reduce the cost of the experimental equipment; however, this is a subject of a separate theoretical study.

At sufficiently large times any diffusion problem yields a stationary solution. Earlier it was shown [11] that the dependence $\ln[R'(\alpha, t)]$ tends to an inclined straight line with the slope equal to the absorption coefficient of the medium μ_a. Having the absorption coefficient determined, one can use the same dependence to find the reduced scattering coefficient of the medium μ_s' [5]. It follows that for a homogeneous object all TPSFs will converge into a single line independent of the detection point [13]. This is important because for a spherical phantom the slope may be calculated independently of the location of the source and detector fibres. For the experiment with a cylindrical phantom all optical fibres should lie in a single plane.

The convergence of all lines $\ln[R'(\alpha, t)]$ to a single straight line indicates that after a certain time t_{iso} the VIS stays in the centre of the phantom [12, 17], which is equivalent to placing the source fibre directly into the centre of the object. This allows direct detection of the inhomogeneity presence in asymmetric cases without solving the inverse problem.

It is important to note, that for an absorbing inhomogeneity the TPSF curves must never intersect [17]. Besides that, the convergence of TPSF logarithms to a single line in the experiments with a homogeneous object provides a test for the correctness of the experiment carried out or for modelling, e.g., using the finite-element method, Monte Carlo method, or analytical calculations. Note, that in a number of publications before papers [12, 17] the necessity of accurate determination of the absolute TPSF intensity and precise time synchronisation of different TPSFs was not taken into account. That is why the curves $\ln[R'(\alpha, t)]$ in earlier papers usually crossed each other.

The second test for the correctness of modelling and experiment is the analysis of an absorbing inhomogeneity. If it is located not in the centre of the symmetric object, then in the logarithmic scale the curves $R'(\alpha, t)$ should converge to parallel lines. This method can be also used for fast detection of inhomogeneities in a variety of asymmetric cases.

The DOT problem is traditionally formulated as follows: a definite distribution of inhomogeneity in the object corresponds to a certain data set. Usually, after this the inverse problem is solved and certain solutions are obtained [13, 19, 20, 22]. Unfortunately, the inverse problem is often solved by step-by-step fitting of the direct problem solution. This could be correct, if the results of finite-element (FEM), Monte Carlo or analytical calculations were compared with those of the experiment. But when the results, obtained by means of FEM, are compared with those of Monte Carlo solution, based on the same diffusion approximation, it is hard not obtain good agreement. Sometimes they even discuss the possibility of millimetre and submillimetre resolution in DOT of biological objects, which is too optimistic, especially taking their high scattering coefficients into account.

Taking into account the characteristic linear dimensions of the object (5–10 cm), the dimensions of the minimal detectable inhomogeneity may be estimated as 5–10 mm. For a cylindrical phantom this is a coaxial cylindrical inhomogeneity inside the main object, for a three-dimensional case this is a spherical inhomogeneity inside a spherical object. Having solved the classical problem of determining the resolution of the measuring device, one can discuss the detection of two, three and more inhomogeneities with different optical properties. At present, when the role of late arriving photons became clear, this problem may be solved by means of numerical modelling, too.

The goal of the present paper is to develop an experimental technique for direct detection of absorbing inhomogeneities in strongly scattering objects using late arriving photons, without reconstruction of the inhomogeneity distribution by solving the inverse scattering problem.

3. Experiment

The experimental setup is shown in Fig. 2. The pulsed radiation from a femtosecond mode-locked Ti : sapphire MIRA 900-B laser (Coherent) is transmitted through a waveguide and is incident on the studied object. The pulsed laser is pumped using radiation from a cw argon INNOVA 307 laser (Coherent). The pulse duration (FWHM) was 100 fs; the wavelength of radiation was 730 nm. The diameter of the source light guiding fibre was 0.5 mm; the diameters of the detector fibres were 0.25 mm.

The role of a phantom was played by a cylinder, made of epoxy resin with the admixture of the titanium dioxide TiO_2 particles with the mean diameter 0.3 μm. The concentration of the particles was chosen such that the reduced scattering coefficient μ_s' was equal to 0.52 mm^{-1}, which corresponds to the scattering coefficient of a biological tissue. The diameter and height of the cylinder were both 68 mm.

To increase the precision of measurements instead of two phantoms, a homogeneous and an inhomogeneous one, we used one phantom, a cylinder with a hole 20 mm in diameter

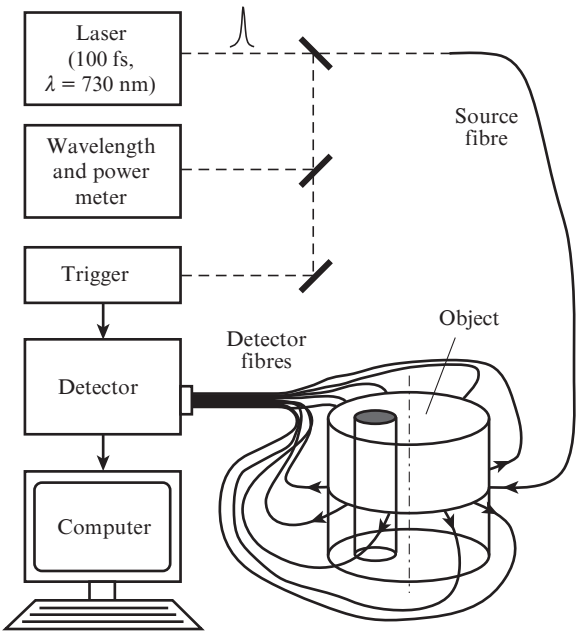

Figure 2. Experimental setup for diffuse optical tomography.

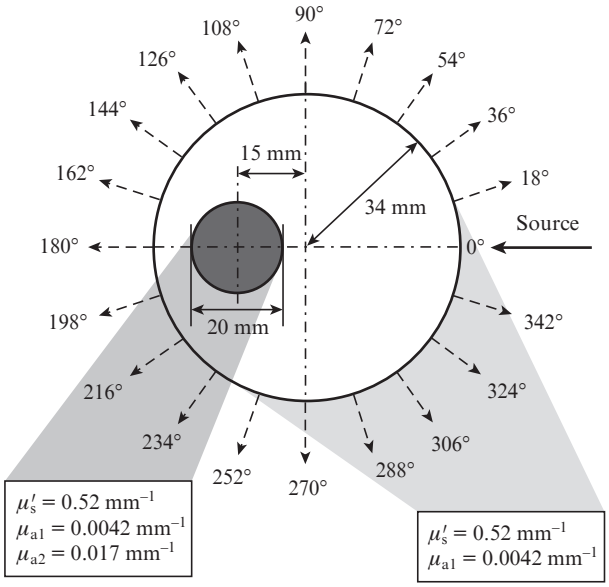

Figure 3. Cross section of the studied cylindrical phantom.

parallel to the axis of the cylinder (Fig. 3). The measurements in a homogeneous phantom were carried out using the small cylinder (with the diameter 20 mm) with the same optical properties ($\mu_s' = 0.52$ mm^{-1}, $\mu_{a1} = 0.0042$ mm^{-1}) as those of the main cylinder. To perform the measurements in an inhomogeneous phantom, a cylinder with a greater absorption coefficient ($\mu_{a2} = 0.017$ mm^{-1}) was introduced into the hole. To model the absorption, a special dye (Indian Ink) with the known spectra of IR absorption was added to the material, from which the cylinder was made.

The detector fibres were arranged in one row and delivered the signal to the Streak Camera C4334 detector array (Hamamatsu Photonics K.K.) with the temporal resolution 10 ps. The measurements of the integral intensity were carried out using the same device, but with the time sweeping switched off. The dynamical range of the detector (10^3–10^4) is essentially lower than that of photomultipliers. This did not allow measurements during one pulse, because the intensity ratio at α = 18° and 180° was or the order of a few millions, which is typical for DOT.

A small fraction of the pulsed radiation was used for simultaneous control of the wavelength and power of the radiation by means of the OMM-6810 multimeter (ILX Lightwave). The other part of radiation arrived at the trigger (a special design by Hamamatsu Photonics K.K.) for synchronisation and triggering of the radiation detector. From the detector the signal was transmitted to the computer for further processing.

The large dynamic range of the detected signal causes serious difficulties in measuring the absolute values of $R'(\alpha, t)$ and $\ln[R'(\alpha, t)]$. Apparently, this was the reason why in earlier papers the signal measured was typically normalised to its maximal value, and the main attention was paid to the shape of TPSF in linear and logarithmic intensity scales [2, 3, 8, 9].

To obtain all curves of the diffused radiation $R(\alpha, t)$ in the same scale and with the account of the absolute intensity, a new two-stage method of measurements was proposed [12]. At the first stage the integrated signal was detected

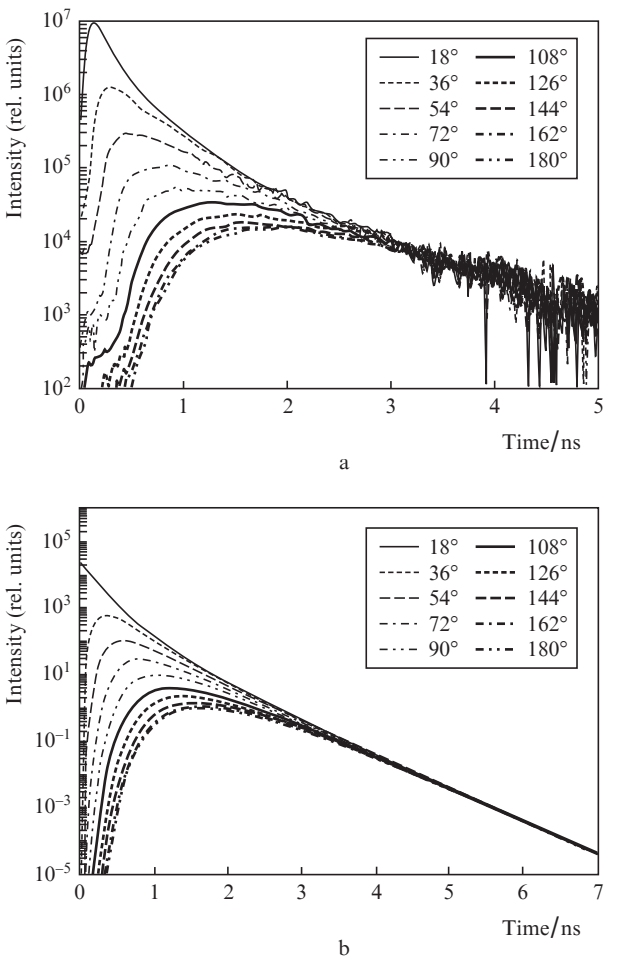

Figure 4. Experimental (a) and calculated (b) intensities of pulsed IR radiation, diffused through a homogeneous phantom and detected at different angles α.

$$T(\alpha) = \int_0^\infty R(\alpha, t)\mathrm{d}t$$

without taking the pulse shape into account. At the second stage only the shape of the diffused pulse was detected (i.e., the time dependence of intensity) with no account for the absolute value of the intensity. The calculation using the formula

$$R(\alpha, t) = T(\alpha)\left(\int_0^\infty R'(\alpha, t)\mathrm{d}t\right)^{-1} R'(\alpha, t)$$

yields the desired distributions of the TPSF intensity for each angle α.

A part of the obtained dependences is shown in Figs 4, 5. It is important to note, that in the inhomogeneous case at the infinity all the curves $\ln[R(\alpha, t)]$ become parallel (Fig. 5a); at that, as mentioned before, $\mu_{a2} > \mu_{a1}$. It is not difficult to show, that in the case of scattering inhomogeneous medium, when $\mu'_{s\,\mathrm{inhom}} > \mu'_{s\,\mathrm{back}}$, the curves will intersect; however, this is a problem to be studied, using 3D FEM or Monte Carlo method.

4. Comparison with modelling

Figures 4b and 5b, c present the results of 3D FEM modelling. The homogeneous and inhomogeneous diffusion problems were solved for the geometry, similar to that of experiment. Figure 4b illustrates the homogeneous case. Apparently, all curves converge into a single line. In Fig. 5b the results for the inhomogeneous case are shown, when the absorbing inhomogeneity is located far from the source fibre (near the fibre with $\alpha = 180°$), and in Fig. 5c the inhomogeneous case is illustrated, when the absorbing inhomogeneity is near the source fibre (near the fibre with $\alpha = 0$). In this case the curves intersect near $t = 2.5–3$ ns and become parallel.

Figure 6 presents the results of calculation of the homogeneity index HI using all TPSFs. This quantity corresponds to the time dependence of the standard deviation of $L(\alpha_i, t) = \ln[R(\alpha, t)]$ from its mean values $\langle L(t)\rangle = N^{-1}\sum_{i=1}^{N} L(\alpha_i, t)$ for N detecting points (in our case $N = 19$) and is calculated using the formula [17]

$$\mathrm{HI}(t) = \left\{\frac{1}{N}\sum_{i=1}^{N}[L(\alpha_i, t) - \langle L(t)\rangle]^2\right\}^{1/2},$$

where α_i is the angle at which the corresponding fibre is located.

In the case of an inhomogeneous object the value of HI(t) tends to zero. In the presence of an inhomogeneity the curves

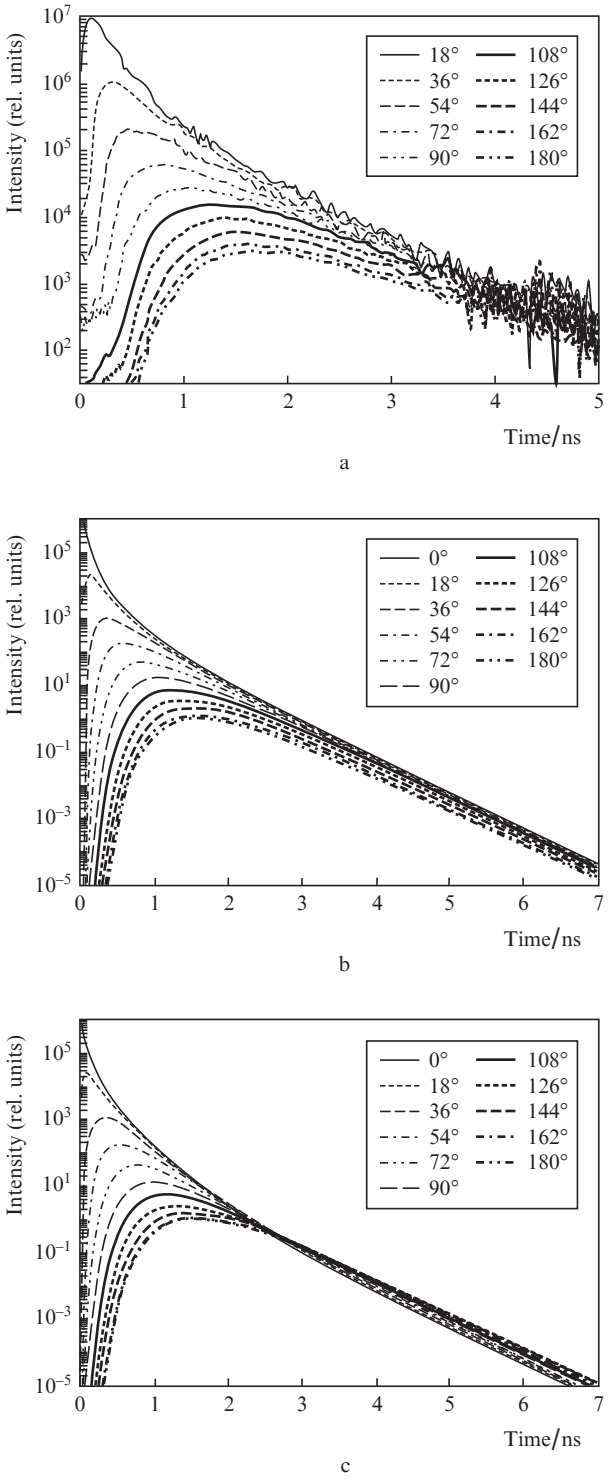

Figure 5. Experimental (a) and calculated (b, c) intensities of pulsed IR radiation, diffused through a phantom with the absorbing inhomogeneity and detected at different angles α; (b) calculation for the inhomogeneity near the fibre with $\alpha = 180°$ (corresponds to Fig. 5a), (c) calculation for the inhomogeneity near the fibre with $\alpha = 0$.

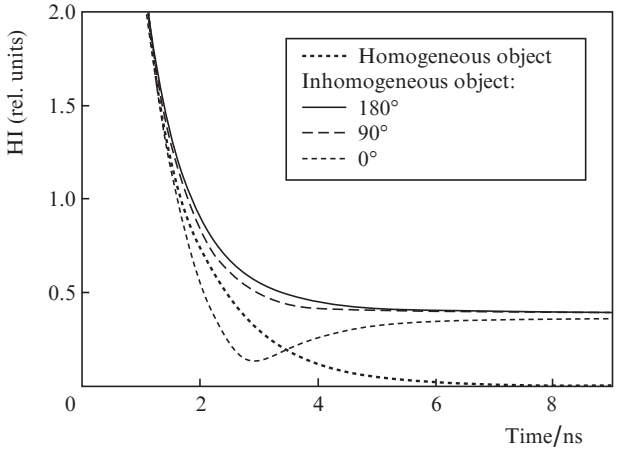

Figure 6. Homogeneity index HI versus time for a homogeneous object and in the presence of inhomogeneity for $\alpha = 180°$, 90°, and 0.

tend to straight lines, parallel to the time axis, and at $\alpha = 0$ the dependence exhibits a minimum.

5. Conclusions

In the situation considered, when the formed virtual isotropic source moves from the surface, after a certain time $t = t_{\text{hom}}$ it is possible to consider it as located in the centre of the phantom, i.e., when registering the late arriving photons, one can assume that the radiation source is placed into the centre of the object. In the case of a moving virtual source the diffusion approximation allows the solution of the DOT problem in two steps: direct detection of the inhomogeneity and restoration of the inhomogeneity distribution map, i.e., the tomography proper.

It is proposed to begin the solution of the DOT problem from finding the difference in time dependent point spread functions at the times, exceeding 2 ns. Then one should proceed to the central part of TPSF, and then to early photons (see Fig. 1).

If one collects all curves into one 3D picture, then in the homogeneous case a plane will appear, while in the inhomogeneous case there will be planes with dips at the angles, near which the inhomogeneity is located. Such a 3D representation will allow direct detection of the presence or absence of an inhomogeneity in real time for the majority of asymmetric cases without solving the inverse problem.

Further research will be concentrated on achieving precise quantitative agreement of the experimental results with those of 3D FEM for a wider class of phantoms, including the case, when the inhomogeneities of different size are located in the centre. For such symmetric phantoms we suggest changing the position of the source fibre with respect to the plane of the detector fibres.

Acknowledgements. The major part of the work was carried out within the framework of the project of two organisations: Bioscience Department of Mechanical Engineering Laboratory and Hamamatsu Photonics K.K., Tsukuba, Japan.

The author expresses his sincere gratitude for the help in this work to his Japanese colleagues Tanikawa Yukari, Takahashi Shuichi, Yamada Yukio from Mechanical Engineering Laboratory and, particularly, to Yamashita Yutaka and Tsuchiya Yutaka from Hamamatsu Photonics K.K.

References

1. Farrell T.J., Patterson M.S. *Med. Phys.*, **19**, 879 (1992).
2. Wang L., Ho P.P., Liu C., Zhang G., Alfano R.R. *Science*, **253**, 769 (1991).
3. Chance B., Nioka S., Kent J., McCully K., Fountain M., Greenfeld R., Holtom G. *Analyt. Biochem.*, **174**, 698 (1988).
4. Proskurin S.G., Yamada Y., Takahashi Y. *Proc. SPIE Int. Soc. Opt. Eng.*, **2389**, 157 (1995).
5. Tsunazawa Y., Oda I., Eda H., Takada M. *Proc. SPIE Int. Soc. Opt. Eng.*, **2389**, 75 (1995).
6. Marquet P., Bevilacqua F., Depeursinge C., de Haller E.B. *Opt. Eng.*, **34**, 2055 (1995).
7. Farrell T.J., Wilson B.C., Patterson M.S. *Phys. Med. Biol.*, **37**, 2281 (1992).
8. O'Leary M.A., Boas D.A., Chance B., Yodh A.G. *Opt. Lett.*, **20**, 426 (1995).
9. Pogue B.W., Patterson M.S., Jiang H., Paulsen K.D. *Phys. Med. Biol.*, **40**, 1709 (1995).
10. Firbank M., Hiraoka M., Delpy D.T. *Proc. SPIE Int. Soc. Opt. Eng.*, **1888**, 264 (1993).
11. Patterson M.S., Chance B., Wilson B.C. *Appl. Opt.*, **28**, 2331 (1989).
12. Proskurin S.G., Tanikawa Y., Kwee I., Yamada Y. *Proc. SPIE Int. Soc. Opt. Eng.*, **2925**, 2 (1996).
13. Arridge S.R., Cope M., Delpy D.T. *Phys. Med. Biol.*, **37**, 1531 (1992).
14. Schweiger M., Arridge S.R., Delpy D.T. *J. Mathem. Im. Vis.*, **3**, 263 (1993).
15. Schweiger M., Arridge S.R., Hiraoka M., Delpy D.T. *Med. Phys.*, **22**, 1779 (1995).
16. Yamada Y., Hasegawa Y. *JSME Int. J. Ser. B*, **39**, 754 (1996).
17. Proskurin S.G., Takahashi S., Kwee I.W., Tanikawa Y., Yamada Y. *Proc. SPIE Int. Soc. Opt. Eng.*, **2979**, 261 (1997).
18. Tsuchiya Y., Ohta K., Urakami T. *Jpn. J. Appl. Phys.*, **34**, 2495 (1995).
19. Gibson A.P., Hebden J.C., Arridge S.R. *Phys. Med. Biol.*, **50**, R1 (2005).
20. Zacharopoulos A.D., Schweiger M., Kolehmainen V., Arridge S. *Opt. Express*, **17**, 18940 (2005).
21. Ripoll J., Schulz R.B., Ntziachristos V. *Phys. Rev. Lett.*, **91**, 1039 (2003).
22. Graber H.L., Xu Y., Pei Y., Barbour R.L. *Appl. Opt.*, **44**, 941 (2005).